Inverse ion-cyclotron damping: Laboratory demonstration and space ramifications[a)]

M. E. Koepke,[b)] C. Teodorescu,[c)] and E. W. Reynolds
Department of Physics, West Virginia University, Morgantown, West Virginia 26506-6315

C. C. Chaston, C. W. Carlson, and J. P. McFadden
Space Sciences Laboratory, University of California, Berkeley, California 94720-7450

R. E. Ergun
Laboratory for Atmospheric and Space Studies, University of Colorado, Boulder, Colorado 80309

(Received 15 November 2002; accepted 12 February 2003)

The familiar and ubiquitous phenomenon of ion-cyclotron damping is shown to be invertible in a laboratory plasma resembling ionospheric plasma in terms of important dimensionless parameters. The ion-cyclotron waves that arise spontaneously appear at all harmonics of the ion-cyclotron frequency, well into the lower-hybrid range. The sign change of the usual ion-cyclotron damping is induced by shear in the magnetic-field-aligned (parallel) ion drift velocity. Full experimental characterization of the wave propagation and particle-velocity distributions are presented to document the case of inverse damping (i.e., growth) and the case in which the damping is significantly reduced. These results support the parallel-velocity-shear interpretation of the multiscale structure observed by the Fast Auroral Snapshot (FAST) satellite. FAST observations of simultaneous shear and multiharmonic ion-cyclotron waves in the upward-current and downward-current regions of the ionosphere (4000-km altitude) are presented and discussed in terms of a new, small-scale analysis of the mechanisms in the auroral region. [DOI: 10.1063/1.1566031]

I. INTRODUCTION

Observations from space-borne instruments are typically interpreted using theoretical models developed to predict the properties and dynamics of geospace.[1] The usefulness of specifically tailored laboratory experiments for providing confirmation of theory by identifying, isolating, and studying physical phenomena efficiently, quickly, and economically has been demonstrated in the past.[2] In this paper, laboratory results verify important aspects of a parallel-velocity-shear mechanism for decreasing and inverting ion-cyclotron damping. This mechanism is one of several that have been used to explain observations of multiharmonic ion-cyclotron waves in space plasma.[3,4] These laboratory results validate the existing theory and therefore contribute to a better understanding of space processes, which cannot be subjected to controlled experimental investigation. Evidence is presented of laboratory-consistent plasma behavior from the Fast Auroral Snapshot (FAST) satellite that supports the parallel-velocity-shear interpretation of the space-observed multi-harmonic ion-cyclotron waves.[5] The laboratory experiments reported here demonstrate the synergistic nature of the scientific alliance between experimentalists making *in situ* space measurements, experimentalists making laboratory measurements, and theorists developing models to describe and predict experiments.[6]

The presence of shear in the magnetic-field-aligned (parallel) drift velocity v_{dz} results in a diamagnetic drift, the free energy of which can be exploited to sustain plasma microinstabilities.[7,8] The shear is expressed dv_{dz}/dr, where the sign of v_{dz} is defined to be positive (negative) if v_{dz} is parallel (antiparallel) to the magnetic field. Each population identifiable by a drift velocity will have an associated value of shear. Also important is the magnitude and sign of the ratio of parallel and perpendicular wave vector components k_z and k_y, respectively, and whether the wave frequency in the drifting-particle frame is slightly above or slightly below the gyrofrequency. In cases where there is a relative phase between different wave components, this phase is useful to know.

II. THEORY OF THE SHEAR-MODIFIED ION-CYCLOTRON INSTABILITY

Attempts to model parallel-velocity shear in a Q-machine plasma were carried out[8] and extended to include kinetic effects,[9] such as resonant-ion damping, magnetic shear, and arbitrary values of T_e/T_i.[10] The electrostatic treatment of parallel-velocity shear for space conditions is discussed[11–15] using a fluid approach by examining modes with frequencies much smaller than the ion gyrofrequency ($\omega \ll \omega_{ci}$). In some fluid treatments, higher-frequency waves ($\omega \approx \omega_{ci}$) were discussed.[16] Gavrishchaka *et al.*[7,17] use a full kinetic model[18] to analyze instabilities that rely on shear in parallel-velocity shear and found a new class of low-frequency ($\omega \ll \omega_{ci}$) solutions associated with ion-acoustic

---

[a)]Paper LI1 2, Bull. Am. Phys. Soc. **47**, 221 (2002).
[b)]Author to whom correspondence should be addressed. Electronic mail: mkoepke@wvu.edu
[c)]Invited speaker.

waves.[19,20] Further investigations[5,21] led to another velocity-shear mode at higher frequency around ω_{ci}.[22] The character of this shear-modified ion-cyclotron instability mechanism is the subject of our recent investigation and is emphasized in this paper. This mechanism makes possible inverse ion-cyclotron damping, as demonstrated here.

The description of the steady state used in the general model[18] includes a uniform magnetic field B that defines the z direction, a magnetic-field-aligned (parallel) relative drift velocity for electrons $v_{dez}(x)$ and ions $v_{diz}(x)$, a localized perpendicular, dc electric field $E_x(x)$, and a density gradient dn/dx. The general eigenvalue condition for this model is[18]

$$\left(\rho_i^2\frac{d^2}{dx^2}-\frac{1+\Sigma F_{ni}(x)\Gamma_n(b)+\tau[1+F_{0e}(x)]}{\Sigma F_{ni}(x)\Gamma_n(b)}\right)\psi(x)=0, \tag{1}$$

where $F_{n\alpha}\equiv A_{n\alpha}-B_{n\alpha}$, $\Gamma_n(b)\equiv I_n(b)\exp(-b)$, $A_{n\alpha}\equiv[(\omega_{1\alpha}+\omega_{2\alpha}-\omega_\alpha^*)/(\sqrt{2}|k_z|v_{t\alpha})]Z[(\omega_{1\alpha}-\omega_{2\alpha}-n\omega_{c\alpha})/(\sqrt{2}|k_z|v_{t\alpha})]$, $B_{n\alpha}\equiv-(\omega_{3\alpha}/(\sqrt{2}|k_z|v_\alpha)]Z'[(\omega_{1\alpha}-\omega_{2\alpha}-n\omega_{c\alpha})/(\sqrt{2}|k_z|v_{t\alpha})]$, I_n are the modified Bessel functions, Z is the plasma dispersion function, $b\equiv(k_y\rho_i)^2$, $\omega_{1\alpha}\equiv\omega k_y v_{d\alpha y}-k_z v_{d\alpha z}$, $\omega_{2\alpha}\equiv k_y v_E''(x)\rho_\alpha^2/2$, $\omega_{3\alpha}\equiv k_y v_{d\alpha}'(x)\rho_\alpha$, ω_α^* is the diamagnetic drift frequency, $v_{t\alpha}\equiv T_\alpha/m\alpha$ is the thermal velocity, $v_{d\alpha}$ is the parallel drift velocity, ρ_α is the ion gyroradius, $\tau\equiv T_i/T_e$, m_α is the mass, α indicates the species (electron or ion), the prime indicates the derivative with respect to the argument, and ψ is the fluctuating electrostatic potential. Neglecting density gradients and perpendicular dc electric fields, $(\omega_{1\alpha}+\omega_{2\alpha}-\omega_\alpha^*)$ becomes $\omega-k_z v_{d\alpha z}$. Equation (1) can be expressed in the local limit[5,7,21] as

$$1+\sum_n \Gamma_n(b)F_{ni}+\tau(1+F_{0e})=0. \tag{2}$$

$$F_{ni}=\frac{\omega_{1i}}{\sqrt{2k_z^2v_{ti}^2}}Z\left(\frac{\omega_{1i}-n\omega_{ci}}{\sqrt{2k_z^2v_{ti}^2}}\right)-\frac{k_y}{k_z}\frac{dv_{diz}/dx}{\omega_{ci}}\left[1+\frac{\omega_{1i}-n\omega_{ci}}{\sqrt{2k_z^2v_{ti}^2}}Z\left(\frac{\omega_{1i}-n\omega_{ci}}{\sqrt{2k_z^2v_{ti}^2}}\right)\right], \tag{3}$$

and

$$F_{0e}=\left(\frac{\omega_{1e}}{\sqrt{2k_z^2v_{te}^2}}\right)Z\left(\frac{\omega_{1e}}{\sqrt{2k_z^2v_{te}^2}}\right)+\frac{k_y}{k_z}\frac{dv_{dez}/dx}{\omega_{ce}}\left[1+\frac{\omega_{1e}}{\sqrt{2k_z^2v_{te}^2}}Z\left(\frac{\omega_{1e}}{\sqrt{2k_z^2v_{te}^2}}\right)\right]. \tag{4}$$

In the absence of shear, Eqs. (2), (3), and (4) revert to the homogeneous-plasma dispersion relation.[23,24]

The solution of the dispersion relation can be expressed as

$$\frac{\omega_{1i}}{\omega_{1i}-n\omega_{ci}}\sigma_{ni}^2\Gamma_n(b)=\frac{T_i}{T_e}\frac{(\omega_{1i}-n\omega_{ci})^2}{k_z^2}\frac{m_i}{k_BT_i}=\frac{T_i}{T_e}\left(\frac{\omega_{1i}-n\omega_{ci}}{k_zv_{ti}}\right)^2, \tag{5}$$

where

$$\sigma_{ni}^2\equiv1-\frac{k_y}{k_z}\frac{dv_{diz}/dx}{\omega_{ci}}\left(1-\frac{n\omega_{ci}}{\omega_{1i}}\right). \tag{6}$$

This yields the following real and imaginary parts of the frequency:

$$(\omega_{1i})_R\approx n\omega_{ci}+\sqrt[3]{\Gamma_n\frac{T_e}{T_i}k_z^2v_{ti}^2\sigma_n^2n\omega_{ci}}, \tag{7}$$

and[21]

$$\frac{(\omega_{1i})_I}{\omega_{ci}}=\frac{\left\{\sqrt{\frac{\tau^3}{m_i/m_e}}\left(\frac{v_{dz}}{(\omega_{1i})_R/k_z}-1\right)-\sum_n\Gamma_n\left[1-\frac{k_ydv_{diz}/dx}{k_z\omega_{ci}}\left(1-\frac{n\omega_{ci}}{(\omega_{1i})_R}\right)\right]\exp\left(-\frac{((\omega_{1i})_R-n\omega_{ci})^2}{2k_z^2v_{ti}^2}\right)\right\}}{\sqrt{\frac{2k_z^2v_{ti}^2}{\pi\omega_{ci}^2}}\sum_{n>0}\frac{4n^2\Gamma_n}{[n^2-(\omega_{1i})_R^2/\omega_{ci}^2]^2}}. \tag{8}$$

The experiment is designed to reach the regime of inverse ion-cyclotron damping that is predicted to be achievable by this model. Ganguli *et al.*[21] express the parallel-velocity-shear dependence of ion-cyclotron damping in terms of a factor σ_{ni} that is unity for the zero-shear case and that can be greater than or less than unity in the presence of shear. For a specific value of shear, there is a ratio of $(1-n\omega_{ci}/\omega_{1i})$ and k_z/k_y that results in zero ion-cyclotron damping. This zero-cyclotron-damping condition is identified with a diagonal line (calculated for the case $dv_{diz}/dx=0.14\omega_{ci}$) in Fig. 1 in which the important regions of parameter space are labeled. For positive shear, the first and third (second and fourth) quadrants in Fig. 1 are associated with reduced (enhanced) ion-cyclotron damping and the diagonal line slants from bottom left to upper right. For negative shear (not shown), the association of the quadrants with reduced and enhanced damping are reversed, with the diagonal line slanting from upper left to bottom right. The points represent a subset of our experimental data and indicate how far from the distinguishing boundaries our cases extend. These cases are elaborated upon later in the paper.

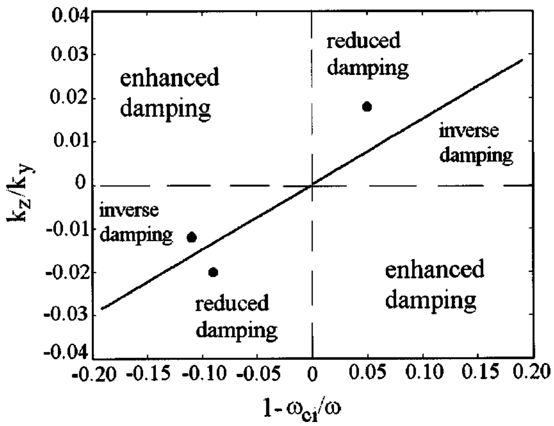

FIG. 1. Regimes of the shear-modified ion-cyclotron wave dispersion relation for fixed shear ($dv_{diz}/dx = 0.14\omega_{ci}$). The three points represent experimental data for which $dv_{diz}/dx = 0.14\omega_{ci}$. The diagonal line corresponds to the ion-cyclotron damping factor equal to zero.

III. DESIGN OF THE LABORATORY EXPERIMENT

We produce plasma that, over a region ten gyroradii or more in diameter, is homogeneous in all respects except for shear in the ion parallel velocity. By incrementing the shear from zero to larger values and measuring the plasma and wave properties, we are able to document, based on the prediction of the theoretical model, reduced and inverted ion-cyclotron damping in the cases that we investigate experimentally.

Experiments are performed in a cylindrical, Q-machine[25] plasma column (6.4 cm diameter, 3 m length, 10^9 cm^{-3} density) radially confined by a uniform, axial magnetic field, typically between 1 and 3 kG. The column is bounded on the left end in Fig. 2 by an ionizer at electrical ground that thermionically emits electrons ($T_e \cong 0.33$ eV) and contact ionizes barium ions ($T_{iz} \cong 0.23$ eV, $T_{iy} \cong 0.26$ eV). The right end in Fig. 2 is bounded by a biased termination electrode. A positively biased annular electrode (3.5 cm outer diameter) is placed 30 cm from the termination electrode and centered on the cylindrical axis. This configuration resembles that used in the original experiments[26] that discovered current-driven electrostatic ion-cyclotron waves, except an annular electrode rather than a disk electrode is used, the annulus is displaced axially rather than coplanar with respect to the termination electrode, and the termination electrode is biased rather than electrically floating. An annulus was used to improve the conditions for azimuthal propagation. The undisturbed boundary condition at the center of a circular button is

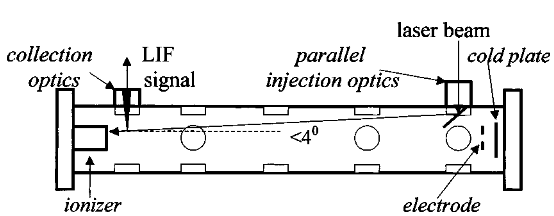

FIG. 2. A schematic of the laser-induced fluorescence parallel injection optics mounted onto the vacuum chamber (not to scale). Angle α is adjustable by rotating the goniometer that aims the laser beam.

believed to favor an $m=0$ azimuthal normal mode with a zeroth-order Bessel function radial mode structure. Removing the center of this electrode is believed to favor the $m=1$ azimuthal normal mode with a first-order Bessel function radial mode structure. The annulus dimensions were chosen so that an $m=1$ normal mode with $k_\perp \rho_i = 1$ would fit the inner circumference and the outer edge would be one gyrodiameter from the plasma-column edge. It was found that the annular electrode and circular button produced waves with similar characteristics except that the annular electrode resulted in waves with large enough amplitude that the components of the wave vector could be measured.

Both electrons and ions drift along the magnetic field from the ionizer toward the electrodes. The magnetic field can be switched to be parallel or antiparallel to the drifts. To connect the experiment's cylindrical geometry to the slab geometry used in the model, z corresponds to the direction of the magnetic field (i.e., both positive and negative drift are possible by reversing **B**), x to the radial direction, and y to the azimuthal direction with positive being clockwise looking parallel to the magnetic field.

The plasma density, measured using a Langmuir probe biased to ion saturation, is approximately 3×10^9 cm^{-3}. The plasma potential, measured using a floating emissive probe, is approximately -3 V. The radial electric field in the plasma is adjusted to be homogeneous ($|E_r| < 10$ V/m) so that the perpendicular $E \times B$ drift speed is negligible compared to the ion thermal speed. The electron parallel-velocity-distribution function is measured with a single-sided Langmuir probe.[27] We observe a single, drifting-Maxwellian population of electrons with a uniform parallel drift speed v_{dez}, even in the presence of parallel-velocity shear. Figure 3 demonstrates the degree of plasma homogeneity in plasma density, emissive-probe floating potential, and electron parallel drift velocity over the central 6-cm-diameter portion of the plasma column. It is evident that the plasma is homogeneous at radii smaller, equal, and larger than the radii associated with the annular electrode, as shown in Fig. 4. Specifically, in the shear layer where the shear-modified ion-cyclotron waves have significant amplitude, the plasma is homogeneous. This homogeneity does not change significantly over the range of shear values, 0% to 20% of ω_{ci}, reported here. The absence of electron velocity shear means dv_{diz}/dx can be measured directly in the laboratory frame.

Note that at the periphery of the plasma column (3 cm $< r < 4$ cm), the electric field is on the order of 100 V/m, whereas throughout $0 < r < 2.5$ cm, the magnitude is on the order of 3 V/m. The observations that we attribute to parallel-velocity shear cannot be attributed to this boundary electric field since, unlike the mode characteristics, this boundary electric field does not change as the velocity shear is varied. Although the region of homogeneous plasma extends more than one gyrodiameter beyond the edge of the annular electrode, an ion that would somehow obtain suprathermal speed in the edge electric field region might be expected to make excursions near the outer edge of the annular electrode, possibly in a region where shear exists. No evidence of suprathermal ions, for example from perpendicular-velocity measurements with laser-induced

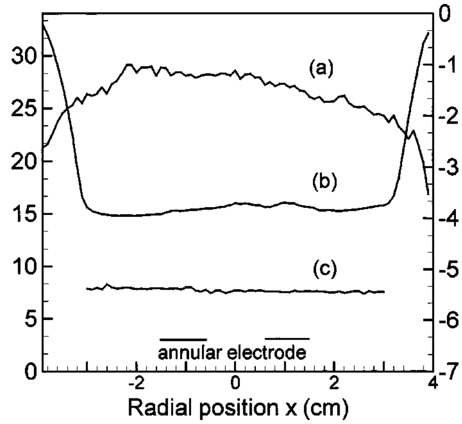

FIG. 3. Radial profiles of (a) plasma density in units of 10^8 cm^{-3} (left-hand scale), (b) emissive-probe floating potential in units of volts (right-hand scale), and (c) parallel electron drift velocity for the parallel-velocity shear case in Fig. 4(a) (circles) in units of $10v_{ti}$ (left-hand scale).

fluorescence, has been found in any region of the plasma, including the region between the annular electrode and the plasma periphery.

Constraints placed on the azimuthal normal-mode geometry by cylindrical effects will restrict the quantity $k_\theta r$ to integer values. Other cylindrical effects will be negligible since the centripetal parameter, $E\times B$ speed divided by $r\omega_{ci}$, is negligible in the vicinity of the shear layer, where r is the radial location being evaluated. In the rotating layer at the periphery, this centripetal parameter is larger but still much smaller than unity.

The ion parallel-velocity-distribution function is measured directly, nonperturbatively, and precisely by laser-induced fluorescence techniques[28] as adopted from the method of Hill *et al.*[29] A hollow-cathode lamp is used for zero-velocity reference. We observe a single drifting-Maxwellian ion population with an adjustable degree of parallel-velocity shear. Parallel-velocity shear is produced and controlled by adjusting the bias V_T on the plasma-column termination electrode (i.e., a nonemitting plasma source) while keeping the applied bias V_0 on the annular electrode fixed. Constant V_0 tends to keep the parallel electron drift velocity constant. It is common to keep V_0 fixed at 35 V (positive), but consistent results are obtained for other values of V_0. Due to a nonzero, but approximately unchanging, degree of alkali–metal contamination of the electrode surface, the effect of an applied bias can be much smaller than the applied bias value might suggest. Shear increases with decreasing bias on the termination electrode. For bias values in the range $V_0-V_T<25$ V, the parallel-velocity shear is negligible. The largest normalized values of shear $(dv_{diz}/dx)/\omega_{ci}$, corresponding to 20% of ω_{ci} ($=125$ krad/s), are obtained for $V_0-V_T=45$ V at 0.2 T. Figure 4(a) shows examples of a flat profile of parallel drift velocity, corresponding to negligible shear, and a sheared profile exhibiting a dip in the central 4 cm diam portion of the plasma column. Figure 4(b) shows the derivative of Fig. 4(a), indicating that the shear layer has a width of approximately 1 cm and a radial position approximately 1 cm from the cylindrical axis. Figure 4(c) presents a few measurements of local, normalized, mode amplitude along the outer region of the radial profile of this quantity, on the basis of which we establish that the mode is associated with the shear layer and not with the strong electric field at the plasma-column periphery. Annular-electrode-averaged measurements of mode amplitude, although providing no shape information on the mode-amplitude profile, provide evidence that it extends to radii smaller than 1.0 cm and to amplitudes larger than 4%. Local measurements of the profile at radii smaller than those reported were not possible without perturbing the plasma to the point of changing the mode-amplitude profile itself.

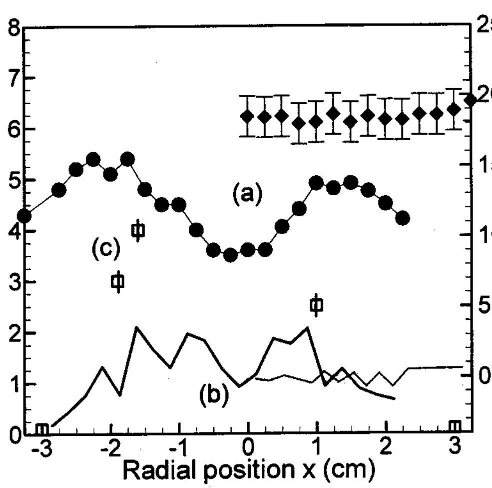

FIG. 4. Radial profiles of (a) parallel drift velocity for shear (circles) and no-shear (diamonds) cases in units of 100 m/s (left-hand scale), (b) parallel-velocity shear for shear (thick line) and no-shear (thin line) cases in (a) in units of (ms)$^{-1}$ (right-hand scale), and (c) mode amplitude for the shear case in units of percent (left-hand scale).

The value of k_z is measured using a two-Langmuir-probe array (separation 3.5 mm) whose tip-to-tip vector's orientation with respect to the magnetic field can be varied 360° by rotating the radially translatable, radially aligned shaft on which the two-tip array is mounted perpendicularly. Fitting to a sinusoid, the relative-phase measurements acquired at numerous values of probe-array orientation angle reduces the uncertainty in the determination of the wave vector compared to the uncertainty of acquiring numerous measurements at a single orientation angle. Precisely incrementing the orientation angle with high resolution over a full rotation sufficiently constrains the magnitude and zero-phase crossing point of the fit that k_z may be determined precisely even with a tip-to-tip spacing much smaller than the axial wavelength. For a very-oblique wave vector (i.e., oriented approximately perpendicular to the magnetic field), the precision of the zero-phase crossing point not only determines the uncertainty in k_z magnitude but also the uncertainty in the sign. The uncertainty in initially referencing the array to the magnetic field ($<\pm1.6°$) is an order of magnitude larger than the uncertainty in subsequently referencing one array orientation to another, and is the dominant contribution to the uncertainty in k_z. Figure 5 plots the tip–tip phase difference in the fluctuating probe signal as a function of the probe-array orientation. The fitted cosine function yields the propa-

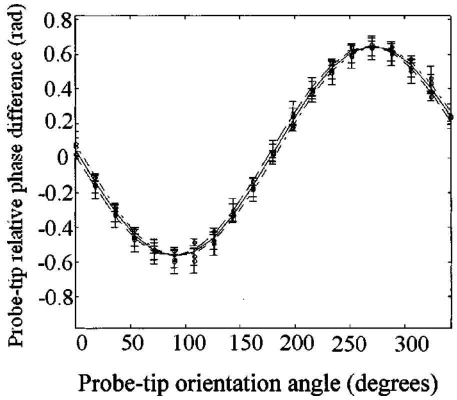

FIG. 5. Probe–tip phase difference as a function of probe orientation and the best-fit cosine function (solid line) yielding $k_z = 0.024\ \mathrm{cm}^{-1}$ and $k_y = -2.210\ \mathrm{cm}^{-1}$. Adjacent lines represent one standard deviation of error from the solid line.

gation angle θ_0, here approximately 90°, and wave vector magnitude, from which $k_y \equiv k \sin \theta_0$, here $(-221 \pm 5)\ \mathrm{m}^{-1}$ and $k_z \equiv k \cos \theta_0$, here $(2.4 \pm 0.4)\ \mathrm{m}^{-1}$. The azimuthal geometry of the mode $e^{im\theta}$ is $m=3$. The k spectrum is narrow compared to the value of k, as shown for both the parallel and perpendicular wave numbers in Fig. 6, indicating that the ion-cyclotron waves are well represented in k space by one dominant Fourier component. The k spectrum is a plot of the fast Fourier transform (FFT) amplitude versus the FFT phase, quantities that are obtained from cross-correlating the two simultaneous signals from the two-Langmuir-probe array. The component of k corresponding to the probe-array orientation is obtained by dividing the relative phase by the probe–tip separation and accounting for the direction of the wave-propagation direction. The probe tips lie on the same magnetic field line in Fig. 6(b) so that k_z can be determined. The probe array is oriented perpendicular to the magnetic field in Fig. 6(b).

IV. PROPERTIES OF THE SHEAR-MODIFIED ION-CYCLOTRON WAVE SPECTRUM

One effect of the parallel-velocity shear is a shear-dependent shift of the wave frequency. This shift is analogous to the shear-induced frequency shift associated with shear-modified ion-acoustic waves.[7,20] Figure 7 shows that the shear-modified ion-cyclotron wave frequency is observed to downshift with increasing shear, consistent with the expectation from the negative derivative of Eq. (7),

$$\frac{\partial \omega_{1i}}{\omega_{1i} \partial(\omega_{ci}^{-1} dv_{diz}/dx)} \approx \frac{k_z^2 c_s^2 \Gamma_n(k_y^2 \rho_i^2)}{2\omega_{1i}^2} \frac{\partial \sigma_{ni}^2}{\partial(\omega_{ci}^{-1} dv_{diz}/dx)} = \frac{k_z^2 c_s^2 \Gamma_n(k_y^2 \rho_i^2)}{2\omega_{1i}^2} \left(-\frac{k_y}{k_z}\right)\left(1 - \frac{n\omega_{ci}}{\omega_{1i}}\right), \tag{9}$$

where it is noted that k_y/k_z is negative and $\omega_{1i} < \omega_{ci}$. The best-fit straight line through the data in Fig. 7 agrees with Eq. (10) within experimental uncertainty, which also reinforces our confidence in the accuracy of the experimental values of ion gyrofrequency and axial wavelength.

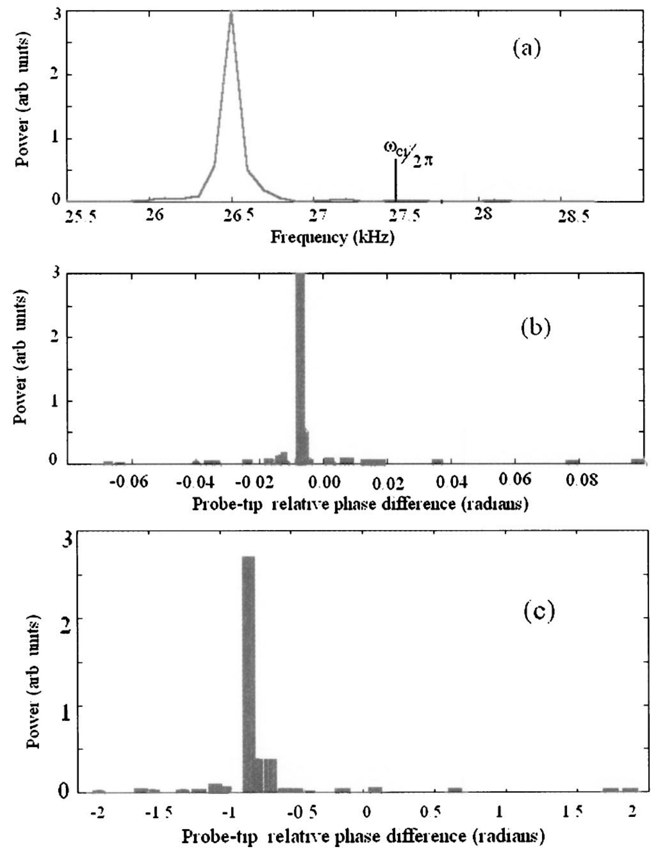

FIG. 6. Shear-modified ion-cyclotron waves. (a) Frequency spectrum, (b) k_z spectrum (probe array is oriented antiparallel to B, thus $k_z = -0.026\ \mathrm{cm}^{-1}$), and (c) k_y spectrum (probe array is oriented 90° to B, thus $k_y = -2.21\ \mathrm{cm}^{-1}$).

As shown in Fig. 8, another shear effect is the appearance of multiharmonic features[30] in the shear-modified ion-cyclotron wave spectrum [Fig. 8(b)], in contrast to the spectra of current-driven electrostatic ion-cyclotron waves [Fig. 8(a)], which typically show a single spectral feature, and sometimes one or two additional harmonics.[31] Figure 9 compares the observed and predicted deviations of each nth harmonic $\omega \cong n\omega_{ci}$ from the nth ion-cyclotron harmonic. The agreement with a linear-theory prediction[5] (open circles) that is independent of n is significantly better than the agreement

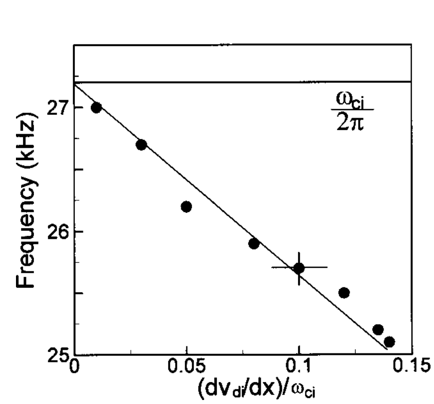

FIG. 7. Downshifting mode frequency ω_{1i} due to parallel-velocity shear. Horizontal line represents the ion-cyclotron frequency and diagonal line represents a best-fit straight line through the experimental points.

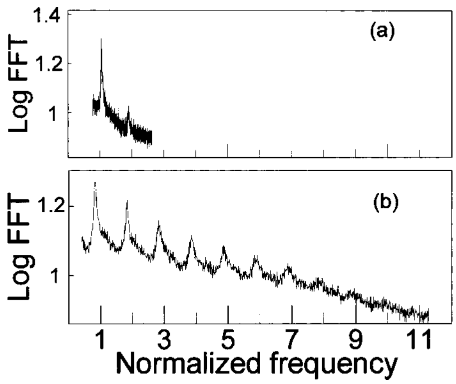

FIG. 8. Fluctuation spectrum of electrostatic ion-cyclotron waves measured from current collected by (a) positively biased button electrode in homogeneous plasma (i.e., without parallel-velocity shear), (b) positively biased Langmuir probe in an inhomogeneous plasma (i.e., with parallel-velocity shear). Fluctuations are normalized to a current-collecting area so that the arbitrary unit in the fast Fourier transform is the same for each spectrum.

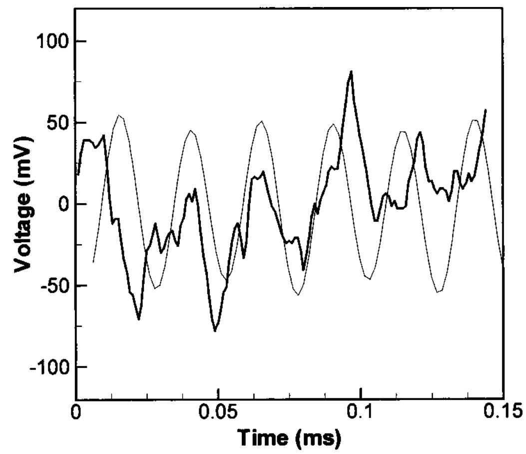

FIG. 10. Fluctuations collected by a Langmuir probe of multiharmonic shear-modified ion-cyclotron waves (thick line) in inhomogeneous plasma (ion-cyclotron damping factor equals 0.38) and single-spectral-feature ion-cyclotron waves (thin line) in homogeneous plasma (damping factor equals unity).

with an n-dependent deviation that is expected if the spectral features are harmonics of the fundamental mode, i.e., nonlinearly coupled. Each spectral feature has associated with it a specific value of $\mathbf{k}$, and thus a specific value of the ion-cyclotron damping factor, as will be quantified in the next section.

The time series associated with shear-modified ion-cyclotron waves is expectedly less sinusoidal than that associated with current-driven ion-cyclotron waves, as shown in Fig. 10. This time series of shear-modified ion-cyclotron waves resembles the spiky, triangle-like fluctuations observed in the parallel electric field from particle-in-cell simulations reported by Gavrishchaka *et al.*[5] in their Fig. 4(c). They pointed out good agreement with observations of parallel electric field from the FAST satellite.[4]

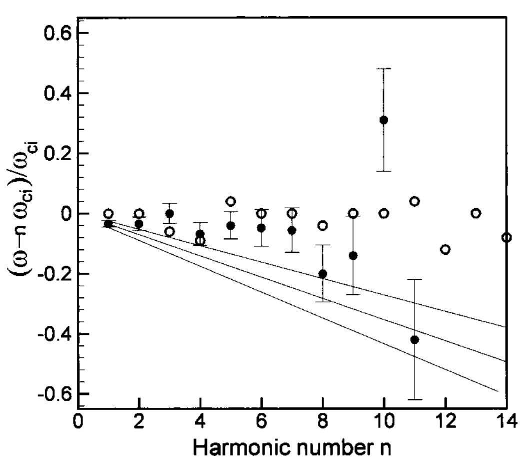

FIG. 9. Deviation of spectral features from the harmonics of the ion-cyclotron frequency. Filled circles correspond to spectral features in Fig. 8, open circles correspond to spectral features in Fig. 2(a) of Ref. 5, and diagonal lines are proportional to deviation at $n=1$ beginning at the $n=1$ datum, at its upper error bar, and at its lower error bar. For the first nine harmonics, the experimental data follow the theoretical prediction associated with linear theory closer than the line associated with coupled harmonics.

V. LABORATORY IDENTIFICATION OF INVERSE CYCLOTRON DAMPING

By reversing the direction of the magnetic field, the sign of the observed shear is likewise reversed. In such cases, associated with enhanced ion-cyclotron damping, no waves are detected for the experimentally realizable values of parallel electron drift velocity, the maximum of which exceeds the current-driven ion-cyclotron wave excitation threshold calculated from homogeneous-plasma theory. Consequently, no determination of the wave vector-component ratio can be made. Nevertheless, this null result suggests that indeed the ion-cyclotron damping for these cases is larger than that in the zero-shear case, assuming no change in the value of k_z/k_y.

Among the cases associated with reduced ion-cyclotron damping, are examples that fall into the inverse ion-cyclotron damping region of Fig. 1. For such a case, a calculation of the ion-cyclotron damping factor for the multiple harmonics yields -0.32, -0.26, -0.19, and -0.25 for harmonic numbers 1, 2, 3, and 4, based on the measured values of the important parameters listed in Table I. The parallel electron drift velocity in this case of inverse ion-cyclotron damping is only 9 km/s, which is $18v_{ti}$. This is considered significantly smaller than the excitation threshold predicted by homogeneous-plasma theory[23,24] for current-driven electrostatic ion-cyclotron waves. The practically ignorable value of electron drift velocity both reinforces the identification of the inverse ion-cyclotron damping regime and suggests that the inverse ion-cyclotron damping is the dominant free-energy mechanism for exciting the shear-modified ion-cyclotron waves in this case.

VI. GEOSPACE CONTEXT

Strong inhomogeneities in parallel current are observed in the Earth's auroral region.[32] The history of this parallel-velocity shear topic began with the laboratory investigation[33]

TABLE I. List of measured quantities used to document inverse ion-cyclotron damping for multiharmonic waves (n is the harmonic number).

n	$(dv_{diz}/dx)/\omega_{ci}$	$k_y(\mathrm{cm}^{-1})/k_z(\mathrm{cm}^{-1})$	$(\omega_{1i})_R\,(\mathrm{krad/s})/n\omega_{ci}(\mathrm{krad/s})$
1	0.14 ± 0.02	$(-2.12\pm0.01)/(0.024\pm0.005)=-88\pm8$	$(156\pm5)/(172.7\pm3.8)=0.903\pm0.006$
2	0.14 ± 0.02	$(-2.35\pm0.02)/(0.028\pm0.005)=-84\pm8$	$(312\pm12)/(345.4\pm11)=0.902\pm0.006$
3	0.14 ± 0.02	$(-2.06\pm0.03)/(0.026\pm0.005)=-79\pm7$	$(468\pm14)/(516\pm13)=0.906\pm0.006$
4	0.14 ± 0.02	$(-2.07\pm0.03)/(0.025\pm0.005)=-83\pm8$	$(623\pm19)/(691\pm18)=0.902\pm0.006$

of a purely growing parallel-velocity-shear instability. The original model,[8] reformulated using kinetic theory,[9] was applied to a variety of space[34] and laboratory[10,35] situations. The original fluid model has been extended to multicomponent and collisional plasma,[14,36] with corresponding experiments.[37–39]

Satellite measurements of parallel-velocity shear have been reported from OGO satellite observations,[11] from HEOS satellite observations,[12] from AE-C satellite observations,[40] from DE-2 satellite observations,[41,42] and recently by the FAST satellite[43] in the upward-current region.[4,5,44] The ω_{ci}-normalized value of parallel-velocity shear associated with the FAST observations is reported to be on the order of 5%.[5]

Gavrishchaka *et al.*[5] show that simultaneous with this level of shear are multiharmonic ion-cyclotron waves, having a power spectrum similar to the multiharmonic, electrostatic, hydrogen-cyclotron waves observed by Kinter *et al.*[3] Ergun *et al.*[4] demonstrate that the electric-field power for these waves is stronger and reaches to more harmonics than does the magnetic-field power. Typical of the FAST data in the shear region are large-amplitude (~500 mV/m), perpendicular-electric-field fluctuations and smaller-amplitude (~200 mV/m), parallel-electric-field fluctuations.

Figures 11(a) and 11(b) present additional FAST-satellite evidence of parallel-velocity shear of this 5% magnitude, here, within the period :13:46 to :13:57 during orbit 1868, with a one-second gap of lower shear at 13:50. Notice that multiharmonic ion-cyclotron waves appear at :13:44, weaken for one second at :13:50, and disappear at :13:55.

Although suggestive of a shear-induced mechanism, the waves appear approximately two seconds before the shear is encountered and at :13:35, the parallel-velocity shear appears unaccompanied by multiharmonic ion-cyclotron waves. Such delays and gaps, although small compared to the 10 s period over which the shear and waves coexist, are attributed to temporal changes in the relative position of the wave-generation region (i.e., the shear region) and the position of the satellite. Because these waves have upward directed Poynting flux,[45] one would expect that a satellite flying above a wave-generation region would observe multiharmonic waves without observing shear, that a satellite flying below a wave-generation region would observe some shear with no waves, and that only a satellite flying through a wave-generation region would observe shear and waves simultaneously. Evidence suggests that the wave amplitude may change more temporally than the shear and this difference may contribute additionally to imperfect synchrony. Nevertheless, the correlation that exists justifies the consideration of the shear-modified ion-cyclotron instability mechanism as another candidate mechanism among other mechanisms[46–52] for explaining multiharmonic ion-cyclotron waves in the upward-current and downward-current regions of the auroral ionosphere.

VII. DISCUSSION AND CONCLUSION

We fully determine the propagation characteristics of multiharmonic ion-cyclotron waves and document cases of both reduced ion-cyclotron damping and ion-cyclotron growth. With the ''wrong''-sign shear, ion-cyclotron damping is enhanced compared to the zero-shear case and the ion-cyclotron waves do not appear. In the ''correct''-sign, large-shear case, the inverse electron Landau damping is perhaps negligible but certainly significantly smaller than in the zero-shear case and the inverse ion-cyclotron damping is apparently the dominant free energy.

Multiharmonic ion-cyclotron waves are observed by the FAST satellite in the upward-current region of the auroral ionosphere, where ion beams are common. As a result of the dramatically structured ionosphere below, the ion beams in the upward-current region can have normalized values of shear that are comparable to the shears produced in the laboratory experiment. The occurrence of the multiharmonic waves in space is correlated with satellite observations of shear in the parallel energy of the ions. Of the three shear periods in Fig. 11, two show the simultaneous appearance and disappearance in both the shear and the multiharmonic ion-cyclotron waves, suggesting that shear is necessary for the generation of these waves. The lack of multiharmonic waves in one of the three shear periods suggests that the satellite is not necessarily flying through the wave-generation region all the time. Two other shear periods, published elsewhere,[4,5] are also consistent with shear being necessary.

The harmonic content of ion-cyclotron waves observed in the downward-current region of the ionosphere by the FAST satellite, as shown in Figs. 12(d) and 12(f), is much smaller than that observed in the upward-current region [Figs. 11(d) and 11(f)]. One observational difference between the two regions is that electron phase-space holes[53] exist in the downward-current region. These electron phase-space holes are sometimes encountered with a clear periodicity of the ion-cyclotron period, in which case their contribution to the observed spectrum is large. Another observational difference between the two regions is that ion beams are not observed in the downward-current region, and therefore sheared ion beams are rare, whereas sheared electron beams are readily found in the downward-current region. According

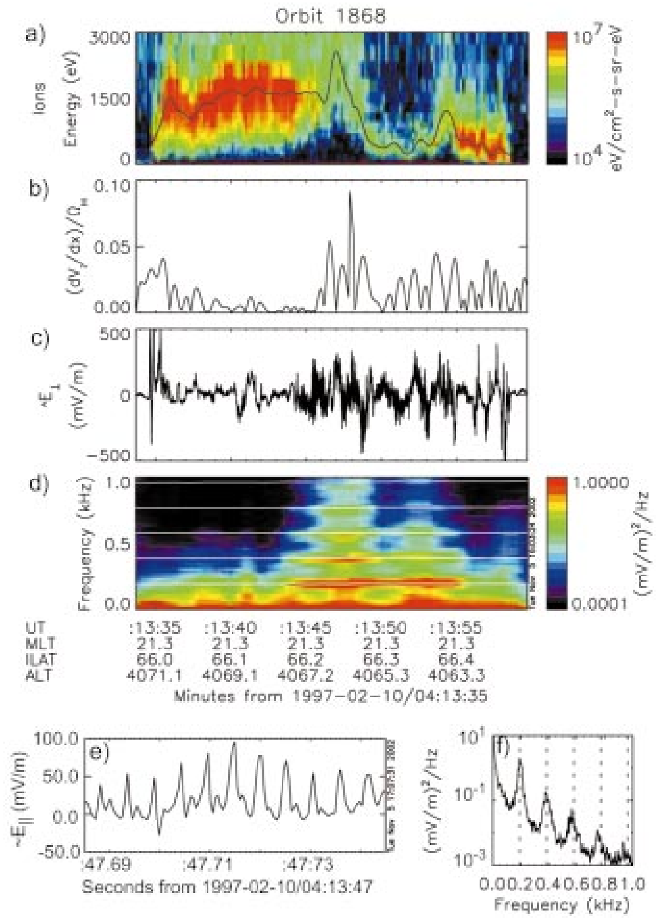

FIG. 11. (Color) Field-aligned ion velocity shear and ion waves in the upward current region. Panel (a) shows the differential energy flux of an upward moving ion beam above the auroral oval. The black trace superimposed on this panel represents the characteristic energy of the beam. Panel (b) shows the normalized shear frequency (the perpendicular gradient in the parallel ion beam velocity) as determined from the characteristic energy trace given in panel (a), the spacecraft position and the proton gyrofrequency. Panel (c) shows the wave electric field measured perpendicular to the geomagnetic field and roughly in the north–south direction. Panel (d) shows the wave power spectrum of the wave field shown in (c) with the white lines indicating harmonics of the proton gyrofrequency. Panel (e) is a snapshot of the wave field component parallel to the geomagnetic field while panel (f) is the averaged spectra from (d), where the average is over the period from :13:45 to :13:50.

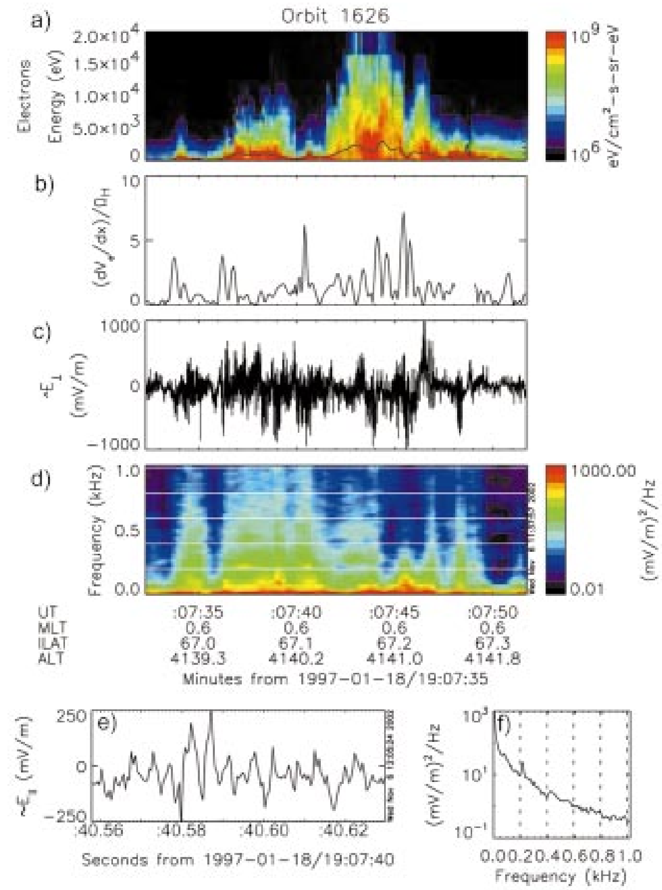

FIG. 12. (Color) Field-aligned electron velocity shear and ion waves in the downward current region. Panel (a) shows the differential energy flux of an upward moving electron beam above the auroral oval. The black trace superimposed on this panel represents the characteristic energy of the beam. Panel (b) shows the normalized shear frequency (the perpendicular gradient in the electron beam velocity) as determined from the characteristic energy trace given in panel (a), the spacecraft position and the proton gyrofrequency. Panel (c) shows the wave electric field measured perpendicular to the geomagnetic field and roughly in the north–south direction. Panel (d) shows the wave power spectrum of the wave field shown in (c) with the white lines indicating harmonics of the proton gyrofrequency. Panel (e) is a snapshot of the wave field component parallel to the geomagnetic field while panel (f) is the averaged spectra from (d), where the average is over the period from :07:36 to approximately :07:42.

to theory, electron-velocity shear and ion-velocity shear, both normalized to the electron and ion gyrofrequency, respectively, and thus are expected to produce different shear effects on ion-cyclotron waves. Consequently, the observation of two-orders-of-magnitude-weaker shear (5% normalized to electron gyrofrequency) in Fig. 12(b), compared to the shear in Fig. 11(b), is expected to yield much smaller multiharmonic-wave activity in Figs. 12(d) and 12(f), compared to Figs. 11(d) and 11(f), which is qualitatively consistent with the diminished multiharmonic-wave activity in Figs. 12(d) and 12(f), compared to the readily apparent multiharmonic-wave activity in Figs. 11(d) and 11(f). Providing laboratory documentation for the case of negligible ion-velocity shear and large electron-velocity shear is a goal of our future laboratory experiments.

ACKNOWLEDGMENTS

We thank V. Gavrishchaka, G. Ganguli, and R. L. Merlino for useful discussions.

This work is supported by the National Science Foundation and by NASA Grant No. NAG5-3596.

[1] D. L. Newman, M. V. Goldman, R. E. Ergun, and A. Mangeney, Phys. Rev. Lett. **87**, 255 001 (2001).

[2] National Research Council, *Plasma Science* (National Academy Press, Washington, DC, 1995), p. 15.

[3] P. M. Kintner, M. C. Kelley, and F. S. Mozer, Geophys. Res. Lett. **5**, 139 (1978); P. M. Kintner, M. C. Kelley, R. D. Sharp, A. G. Ghielmetti, M. Temerin, C. A. Cattell, and P. Mizera, J. Geophys. Res. **84**, 7201 (1979).

[4] R. E. Ergun, C. W. Carlson, J. P. McFadden, F. S. Mozer, G. T. Delory, W. Peria, C. C. Chaston, M. Temerin, R. Elphic, R. Strangeway, R. Pfaff, C. A. Cattell, D. Klumpar, E. Shelley, W. Peterson, E. Moebius, and L. Kistler, Geophys. Res. Lett. **25**, 2025 (1998).

[5] V. V. Gavrishchaka, G. I. Ganguli, W. A. Scales, S. P. Slinker, C. C. Chaston, J. P. McFadden, R. E. Ergun, and C. W. Carlson, Phys. Rev. Lett. **85**, 4285 (2000).

[6]M. E. Koepke, Jpn. J. Plasma Fusion Res. **78**, 721 (2002).
[7]V. Gavrishchaka, S. Ganguli, and G. Ganguli, Phys. Rev. Lett. **80**, 728 (1998).
[8]N. D'Angelo, Phys. Fluids **8**, 1748 (1965).
[9]C. G. Smith and S. von Goeler, Phys. Fluids **11**, 2665 (1968).
[10]P. J. Catto, M. N. Rosenbluth, and C. S. Liu, Phys. Fluids **16**, 171 (1973).
[11]N. D'Angelo, J. Geophys. Res. **78**, 1206 (1973).
[12]N. D'Angelo, A. Bahnsen, and H. Rosenbauer, J. Geophys. Res. **79**, 3129 (1974).
[13]T. A. Potemra, J. P. Doering, W. K. Peterson, C. O. Bostrom, R. A. Hoffman, and L. H. Brace, J. Geophys. Res. **83**, 3877 (1978).
[14]B. Basu and B. Coppi, J. Geophys. Res. **94**, 5316 (1989).
[15]P. K. Shukla, G. T. Birk, and R. Bingham, Geophys. Res. Lett. **22**, 671 (1995).
[16]P. K. Shukla and L. Stenflo, Plasma Phys. Rep. **25**, 355 (1999).
[17]V. V. Gavrishchaka, S. B. Ganguli, and G. I. Ganguli, J. Geophys. Res. **104**, 12 683 (1999).
[18]G. Ganguli, M. J. Keskinsen, H. Romero, R. Heelis, T. Moore, and C. Pollock, J. Geophys. Res. **99**, 8873 (1994).
[19]E. Agrimson, N. D'Angelo, and R. L. Merlino, Phys. Rev. Lett. **86**, 5282 (2001).
[20]C. Teodorescu, E. W. Reynolds, and M. E. Koepke, Phys. Rev. Lett. **88**, 185 003 (2002).
[21]G. Ganguli, S. Slinker, V. Gavrishchaka, and W. Scales, Phys. Plasmas **9**, 2321 (2002).
[22]C. Teodorescu, E. W. Reynolds, and M. E. Koepke, Phys. Rev. Lett. **89**, 105 001 (2002).
[23]W. E. Drummond and M. N. Rosenbluth, Phys. Fluids **5**, 1507 (1962).
[24]J. M. Kindel and C. F. Kennel, J. Geophys. Res. **76**, 3055 (1971).
[25]N. Rynn and N. D'Angelo, Rev. Sci. Instrum. **31**, 1326 (1960); M. E. Koepke, J. J. Carroll III, and M. W. Zintl, Phys. Plasmas **5**, 1671 (1998).
[26]R. W. Motley and N. D'Angelo, Phys. Fluids **6**, 296 (1963).
[27]E. A. Bering, M. C. Kelley, F. S. Mozer, and U. V. Fahleson, Planet. Space Sci. **21**, 1983 (1973); W. Gekelman and R. L. Stenzel, Phys. Fluids **21**, 2014 (1978).
[28]M. E. Koepke, M. W. Zintl, C. Teodorescu, E. W. Reynolds, G. Wang, and T. N. Good, Phys. Plasmas **9**, 3225 (2002).
[29]D. N. Hill, S. Fornaca, and M. G. Wickham, Rev. Sci. Instrum. **54**, 309 (1983).
[30]E. Agrimson, N. D'Angelo, and R. L. Merlino, Phys Lett A **293**, 260 (2002).
[31]J. J. Rasmussen and R. W. Schrittwieser, IEEE Trans. Plasma Sci. **19**, 457 (1991).
[32]K. Stasiewicz and T. Potemra, J. Geophys. Res. **103**, 4315 (1998).
[33]N. D'Angelo and S. von Goeler, Phys. Fluids **9**, 309 (1966).
[34]S. B. Ganguli and P. J. Palmadesso, J. Geophys. Res. **92**, 8673 (1987); S. B. Ganguli and V. V. Gavrishchaka, *ibid.* **106**, 25 601 (2001).
[35]D. R. McCarthy, J. F. Drake, and P. N. Guzdar, Phys. Fluids B **5**, 2145 (1993); D. R. McCarthy, A. E. Booth, J. F. Drake, and P. N. Guzdar, Phys. Plasmas **4**, 300 (1997).
[36]N. D'Angelo and B. Song, IEEE Trans. Plasma Sci. **19**, 42 (1991).
[37]B. Song, D. Susczynsky, N. D'Angelo, and R. L. Merlino, Phys. Fluids B **1**, 2316 (1989).
[38]T. An, R. L. Merlino, and N. D'Angelo, Phys. Lett. A **214**, 47 (1996).
[39]J. Willig, R. L. Merlino, and N. D'Angelo, J. Geophys. Res. **102**, 27 249 (1997).
[40]T. A. Potemra, J. P. Doering, W. K. Peterson, C. O. Bostrom, R. A. Hoffman, and L. H. Brace, J. Geophys. Res. **83**, 3877 (1978).
[41]R. A. Heelis, J. D. Winningham, M. Sugiura, and N. C. Maynard, J. Geophys. Res. **89**, 3893 (1984).
[42]M. Loranc, W. B. Hanson, R. A. Heelis, and J.-P. St. Maurice, J. Geophys. Res. **96**, 3627 (1991).
[43]C. W. Carlson, R. F. Pfaff, and J. G. Watzin, Geophys. Res. Lett. **25**, 2013 (1998).
[44]J. P. McFadden, C. W. Carlson, R. E. Ergun, F. S. Mozer, M. Temerin, W. Peria, D. M. Klumpar, E. G. Shelley, W. K. Peterson, E. Moebius, L. Kistler, R. Elphic, R. Strangeway, C. Cattell, and R. Pfaff, Geophys. Res. Lett. **25**, 2021 (1998).
[45]G. C. Chaston, R. E. Ergun, G. T. Delory, W. Peria, M. Temerin, C. Cattell, R. Strangeway, J. P. McFadden, C. W. Carlson, R. C. Elphic, D. M. Klumpar, W. K. Peterson, E. Moebius, and R. Pfaff, Geophys. Res. Lett. **25**, 2057 (1998).
[46]D. J. Knudsen and J.-E. Wahlund, J. Geophys. Res. **103**, 4157 (1998).
[47]P. Norqvist, M. Andre, and M. Tyrland, J. Geophys. Res. **103**, 23 459 (1998).
[48]M. Andre, P. Norqvist, L. Andersson, L. Eliasson, A. I. Eriksson, L. Blomberg, R. E. Erlandson, and J. Waldenmark, J. Geophys. Res. **103**, 4199 (1998).
[49]C. Cattell, R. Bergmann, K. Sigsbee, C. Carlson, C. Chaston, R. Ergun, J. McFadden, F. S. Mozer, M. Temerin, R. Strangeway, R. Elphic, L. Kistler, E. Moebius, L. Tang, D. Klumpar, and R. Pfaff, Geophys. Res. Lett. **25**, 2053 (1998).
[50]E. J. Lund, E. Moebius, C. W. Carlson, R. E. Ergun, L. M. Kistler, B. Klecker, D. M. Klumpar, J. P. McFadden, M. A. Popecki, R. J. Strangeway, and Y. K. Tung, J. Atmos. Sol.-Terr. Phys. **62**, 467 (2000).
[51]D. L. Newman, M. V. Goldman, and R. E. Ergun, Phys. Plasmas **9**, 2337 (2002).
[52]C. Cattell, L. Johnson, R. Bergmann, D. Klumpar, C. Carlson, J. McFadden, R. Strangeway, R. Ergun, K. Sigsbee, and R. Pfaff, J. Geophys. Res. **107**, SMP 12 (2002).
[53]R. E. Ergun, Y.-J. Su, L. Andersson, C. W. Carlson, J. P. McFadden, F. S. Mozer, D. L. Newman, M. V. Goldman, and R. J. Strangeway, Phys. Rev. Lett. **87**, 045003 (2001).